colloids and interfaces

MDPI

Article

Formulating Graphite-Filled PU Dispersions with Extended Shelf Life Using the Capillary Suspension Concept

Katrin Dyhr * and Norbert Willenbacher

Karlsruhe Institute of Technology, Institute for Mechanical Process Engineering and Mechanics, Gotthard-Franz-Straße 3, 76131 Karlsruhe, Germany; norbert.willenbacher@kit.edu
* Correspondence: katrin.dyhr@kit.edu

Abstract: Stabilizing micron-sized particles in low-viscosity polymer dispersions is challenging when density differences are present. This study demonstrates that graphite particles in aqueous polyurethane dispersions can be efficiently prevented from sedimentation using the capillary suspension concept. Capillary suspensions are solid/liquid/liquid systems and the capillary forces inferred from adding a second immiscible fluid can lead to drastic changes in texture and flow. Here, both spherical and flake-shaped graphite particles were used as fillers, with octanol as the secondary liquid. At low graphite concentrations, octanol increases the low-shear viscosity significantly attributed to the formation of loose particle aggregates immobilizing part of the continuous phase. Above a critical graphite concentration, capillary forces induce a self-assembling, percolating particle network, leading to a sharp yield stress increase (>100 Pa). The corresponding percolating particle network efficiently suppresses sedimentation; for the system including 28 vol% spherical particles, a shelf life of at least six months was achieved. Capillary forces do not affect the high-shear viscosity of suspensions; here, a hydrophobically modified polyether thickener can be used. Transfer of the stabilization concept presented here to other high-density particles like silver or metal oxides suspended in other polymer dispersions is straightforward and is applicable in various fields like flexible printed electronics.

Keywords: capillary suspension; aqueous polymer dispersion; electrically conductive adhesive; sedimentation suppression

Academic Editors: To Ngai and Reinhard Miller

Received: 20 March 2025
Revised: 19 April 2025
Accepted: 30 April 2025
Published: 2 May 2025

Citation: Dyhr, K.; Willenbacher, N. Formulating Graphite-Filled PU Dispersions with Extended Shelf Life Using the Capillary Suspension Concept. *Colloids Interfaces* **2025**, *9*, 26. https://doi.org/10.3390/colloids9030026

1. Introduction

Aqueous polymer dispersions, including polyurethane (PU) dispersions, are widely used in various industries because they are environmentally friendly. Where possible, solvent-based paints are replaced with aqueous polymer dispersions that either have a very low content of volatile organic compounds (VOCs) or are VOC-free [1,2]. Furthermore, polymer dispersions are characterized by their low viscosity at high solids content compared to polymer solutions, which facilitates easy handling and processing [3,4]. Complex formulations based on such polymer dispersions are used, e.g., in the construction, automotive, textile, or electronic industry as coatings, sealants, or as adhesives with an annual production in the order of 10 million tons [5–9].

In most applications, active ingredients or fillers are added to achieve specific features such as color, electrical or thermal conductivity, or simply to reduce cost. Polymer dispersions with suitable conductive fillers can thus be utilized as thermally or electrically conductive adhesives or in flexible electronics, an area experiencing increasing demand [8,10,11]. These formulations typically consist of a solvent, a polymeric binder, and a conductive filler.

Silver is a commonly used filler due to its high conductivity; however, in applications where a high conductivity is not required, cost-effective graphite serves as a viable alternative for flexible electronics [12–14].

Nevertheless, sedimentation of active materials like graphite or fillers with a density generally much larger than the aqueous dispersion and a particle size typically in the order of several microns can lead to an undesired short shelf life. This effect can be counteracted by introducing a yield stress, which can be achieved using associative thickeners such as hydrophobically modified polyurethanes (HEUR) or polyether (HMPE), creating a yield stress and increasing the viscosity by forming polymer networks [2,15,16], which may or may not incorporate the suspended particles. The yield stress required to prevent settling is directly proportional to the density difference between the particles and surrounding liquid as well as the particle diameter [17–19].

Another method to establish a yield stress is through the capillary suspension concept [20]. Capillary suspensions are ternary solid/liquid/liquid systems where the addition of a small amount of an immiscible secondary liquid leads to the formation of a strong self-assembling, sample-spanning particle network. Due to this particle network, a yield stress is observed and typically can be adjusted in a wide range depending on the type and fraction of the secondary liquid [20–22]. Capillary suspensions exist either in the pendular state, when the secondary liquid preferentially wets the particles, or in the so-called capillary state, when the secondary fluid does not wet the particles [20]. The network strength is controlled by the interfacial tension between the two included liquids and by the three-phase contact angle Θ of the secondary liquid on the particle surface. The yield stress of a capillary suspension of monodisperse spherical particles of radius r in the pendular state ($\Theta < 90°$) is given as $\sigma_y = f(\phi_p) 2\pi\Gamma cos\Theta / r$ [23].

Where the pre-factor $f(\phi_p)$ is determined not only by the particle volume fraction, but also by the coordination number, i.e., the number of liquid bridges per particle. The number of bridges may depend on the amount of secondary liquid available to the particles for forming pendular bridges. Typically, three regimes in network strength are observed dependent on φ_s/φ_p, denoting the ratio of the secondary liquid volume fraction φ_s to the particle volume fraction φ_p. Initially, i.e., at low φ_s/φ_p, there is a strong increase in yield stress as network structures form and a percolating particle network is established. This is followed by a plateau in σ_y until the particle network becomes oversaturated, leading to a spherical agglomerate, which weakens the network structure and hence σ_y decreases. For particle flakes, the yield stress plateau sets in at a higher φ_s/φ_p and the absolute yield stress values are higher because the liquid bridges can accommodate a larger volume before becoming oversaturated [23].

Capillary suspensions offer a promising way to adjust dispersion rheology without or reduced need of non-volatile polymeric additives, which may disturb the end-use properties of the product [24]. Moreover, capillary suspensions exhibit a strong degree of shear thinning and a fast structural recovery after the cessation of flow, which makes them ideally suited for many coating or printing applications such as screen printing [25] and dispensing- or extrusion-based additive manufacturing [26–29]. Consequently, capillary suspensions have been utilized to control the stability and flow behavior of solar cell metallization pastes [24,25], battery slurries [30,31], or food suspensions [32,33]. Particle networks stabilized by capillary forces typically exhibit a much higher strength than particulate gels controlled by attractive van der Waals interactions, allowing the main fluid to be removed without significant changes in the network structure. For example, for macro porous ceramics and glasses with an exceptionally high open porosity and corresponding superior filtration performance, and when functional ceramics are employed, unusual piezoelectric properties can be achieved this way [34,35]. Sample-spanning particle networks

controlled by capillary forces may form even at low particle concentrations of about 5 vol% and if conductive particles are used, the percolation threshold for thermal or electrical conductivity can be significantly reduced, compared to corresponding binary suspensions, as first demonstrated for a thermally conductive adhesive based on an epoxy resin designed for chip packaging applications [36]. Capillary forces can also induce percolating particle networks in ternary blends of silica and two immiscible polymers [22] and have even been used to stabilize liquid foams [37].

So far, the benefits of the capillary suspension concept have been demonstrated for a wide range of particle–liquid–liquid systems. However, in complex fluids including active material fillers, as well as polymer dispersions, both the active ingredient or filler and the polymer are present in particulate form. The applicability of the capillary suspension concept to these systems remains unproven, and the interaction between the secondary liquid and both particulate phases is not yet clearly understood. Therefore, this study aims to determine whether the capillary suspension concept can be applied to such complex fluids including micron-sized active material or filler particles as well as nano-scale polymer particles. To stabilize the typically high-density, micron-sized particles using the capillary suspension concept, the secondary liquid should show only minimal interaction with the polymer particles, while forming a strong network with the active ingredient or filler. Particularly, the secondary fluid should not be trapped swelling the polymer particles. Here, we use graphite-filled PU dispersion as a model system, since graphite is widely used as a conductive filler. Roundish, almost spherical and flake-like micron-sized graphite particles were dispersed in a nano-sized PU dispersion, and octanol was added as a secondary liquid. The samples were rheologically characterized using viscosity and yield stress measurements to validate particle aggregation and the formation of a capillary suspension. Sedimentation tests were carried out to demonstrate the shelf life of the samples. In addition, graphite–PU films were produced, and their electrical conductivity as well as their mechanical strength was characterized in order to evaluate whether the secondary liquid and the microstructure of the distinct particle network in the wet state affect the properties of the final dry film.

2. Materials and Methods

2.1. Materials

The aqueous PU dispersion Dispercoll U 53 (Covestro AG, Leverkusen, Germany) with an average particle diameter of $x_{50,3}$ = 150 ± 4 nm measured with Zetasizer Nano ZS (Malvern Instruments, Worcestershire, UK) was used as the main fluid. The secondary liquid utilized here was n-octanol (Merck KGaA, Darmstadt, Germany). Rheovis PE 1330 (BASF SE, Ludwigshafen am Rhein, Germany) was employed as an associative thickener. The synthetic graphite powder of roundish, approximately spherical particles MGP-A utilized here was purchased from China Steel Chemical Corporation (Kaohsiung, Taiwan), while the flake-like particles GFG20 were provided by SGL Carbon SE (Wiesbaden, Germany). SEM images showing the morphology of the particles are found in Figure 1.

The equivalent sphere diameter of the particles given in Table 1 were characterized using a HELOS H0309 laser diffraction instrument (Sympatec GmbH, Clausthal-Zellerfeld, Germany).

Table 1. Particle size x and density ρ of particles used in this study.

	Spherical	**Flakes**
$x_{10,3}/\mu m$	5.3	5.1
$x_{50,3}/\mu m$	21.1	20
$x_{90,3}/\mu m$	30.2	56.3
$\rho/g/cm^3$	2.22 ± 0.01	2.27 ± 0.07

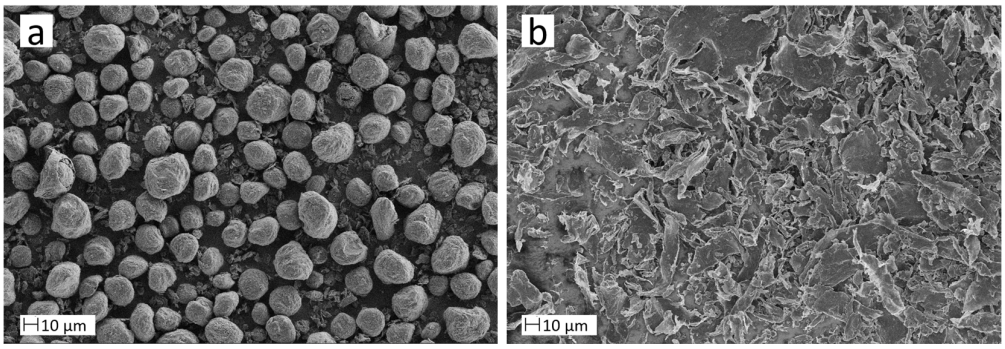

Figure 1. SEM image of (**a**) roundish, spherical graphite particles and (**b**) graphite flakes used in this study.

2.2. Interfacial Properties

To determine the interfacial properties, pendant and sessile drop methods were applied. For the interfacial tension measurements, a drop of PU dispersion was dispensed using a hollow needle (diameter d = 1.8 mm) into a glass cuvette filled with octanol. For the three-phase contact angle measurements, a graphite plate (3 cm × 3 cm × 1 cm) was immersed in water and placed on placeholders. Octanol was dispensed beneath the plate surface. Three-phase wetting angles of the sessile drops were evaluated using the tangent method. Interfacial tension and three-phase contact angle values were calculated using commercially available software (drop shape analysis, Krüss GmbH, Hamburg, Germany).

2.3. Sample Preparation

The samples were prepared at room temperature using a planetary centrifugal mixer (Speedmixer DAC 150, Hauschild GmbH & Co. KG, Hamm, Germany). Initially, the graphite powder and PU dispersion were mixed for 2 min at 2000 rpm. After the addition of octanol and if applicable of the thickening agent, another mixing step was performed under the same conditions. For samples with flake-shaped particles, an additional 4 min mixing at 1000 rpm was conducted with the addition of ceramic hard balls with a diameter of 5 mm to produce homogeneous, agglomerate-free pastes. The volume fractions specified in this work were determined gravimetrically.

The films were prepared using rectangular frames with an inner width of 50 mm, a length of 65 mm, and a thickness of 1 mm for electrical conductivity measurements and 2 mm for tensile tests. The frames were placed on a silicon mat and filled with the sample using a squeegee. The samples were then dried at 60 °C for at least 12 h to ensure the formation of a homogeneous film. The corresponding particle loading of the film was calculated with the assumption that water and secondary liquid totally evaporate during the drying process.

2.4. Rheological Characterization

A rotational rheometer (Haake MARS, Thermo Fisher Scientific, MA, USA) was used to determine the viscosity η and yield stress σ_y of the prepared samples at 20 °C. In order to determine η, rate-controlled measurements were carried out, increasing the shear rate from 0.1 s^{-1} to 1000 s^{-1} in 24 logarithmic steps at a duration of 8 s per step, followed by a stepwise decrease in the shear rate from 1000 s^{-1} to 0.1 s^{-1} in a similar way. A plate–plate geometry with a diameter of 35 mm was used for all viscosity measurements except for measuring the viscosity of the PU dispersion without thickener and graphite. In this case, a Couette system with a 20 mm diameter inner cylinder was used. For yield stress determination, the shear stress was stepwise increased from 0.1 to 1000 Pa in 41 logarithmic steps with 5 s duration per step, and deformation was measured. The data

were depicted in a double-logarithmic strain–stress diagram. For yield stress fluids, these γ vs. σ curves exhibit an initial branch with slope 1 corresponding to the elastic response regime at $\sigma < \sigma_y$, followed by a sharp kink and a branch showing a much stronger slope. The yield stress was then determined according to the tangent intersection method [38]. Each sample was measured three times, and the average and standard deviations were calculated. Additionally, experimental uncertainties due to variations in sample preparation were estimated.

Frequency sweeps were performed using a Couette system with an inner cylinder of 20 mm diameter. The stress amplitude was selected from the linear viscoelastic (LVE) range, as determined previously through amplitude sweeps. The frequency was increased from 0.01 s^{-1} to 10 s^{-1}.

Amplitude sweeps were conducted using a rotational rheometer (Physica, MCR 501, Anton Paar Germany GmBH, Ostfildern-Scharnhausen, Germany) to evaluate the yield stress in an alternative way. A plate–plate geometry with a 50 mm diameter was employed, and a constant frequency of 10 s^{-1} was set. The stress amplitude was varied from 0.01 to 100 Pa for samples expected to exhibit a yield stress below 10 Pa, and from 0.1 to 1000 Pa for samples anticipated to have a higher yield stress. Yield stress was determined as the stress amplitude value where the storage modulus deviated by 10% from the plateau within the linear viscoelastic (LVE) range as suggested in [38].

2.5. Electrical Characterization

Films with a thickness of 1 mm in the wet state were cut into 8 mm strips. To calculate the conductivity, the resulting thickness of the sample was determined. Three measurements per strip were taken using a four-point measurement with a 2450 SourceMeter (Keithley, OH, USA) at a current of 10 mA.

2.6. Mechanical Characterization

The dog bone specimen for tensile tests was punched out of films. The measuring length was 20 mm, and the width 4 mm. The thickness resulted from a 2 mm thick wet film layer and was approximately 1.1 $\pm$ 0.2 mm. At least 6 tensile test specimens were characterized for each composition. The tensile tests were carried out using a TA.XT plus Texture Analyzer (Stable Micro Systems, Godalming, UK) at a test speed of 0.01 mm/s.

3. Results and Discussion

3.1. Graphite Particles Suspended in a PU Dispersion

The systems investigated in this work are based on a PU dispersion including 35 vol% of nano-scale PU particles as the main or bulk liquid phase, micron-sized spherical or flake-like graphite particles as the solid phase, and octanol as the secondary liquid. The capillary force in such ternary systems scales with $\Gamma\cos\Theta$; here, Γ = 5.6 $\pm$ 0.1 mN/m and Θ = 12 $\pm$ 2. The three-phase contact angle of octanol on graphite was determined here in the presence of water. The opaque aqueous PU dispersion was unsuitable for the optical determination of the three-phase contact angle and since it may contain amphiphilic additives, this value has to be considered as an approximation, but obviously octanol wets graphite very well and if a capillary suspension is formed, it is supposed to be in the pendular state.

3.1.1. Effect of Octanol Below Percolation Threshold

To evaluate if the capillary suspension concept can be adapted to graphite-filled PU dispersions, we first consider the effect of octanol on the viscosity and the storage and loss moduli of the PU dispersion filled with 3.7 vol% of flake-like graphite particles. Figure 2a shows the viscosity as a function of the shear stress and b) demonstrates the storage

modulus G′ and loss modulus G″ in dependence of the angular frequency $\omega = 2\pi f$ for different amounts of added octanol, the ratio of the volume fraction of secondary liquid to the solid phase φ_s/φ_g is varied between 0 and 0.4, and the viscosity of the pure PU dispersion with and without added octanol is shown for reference. Note that the symbol φ_g refers to the volume fraction of the graphite particles only; the PU particles are not included here, since we assume that they do not contribute to the particle network controlled by the capillary forces due to the added secondary liquid.

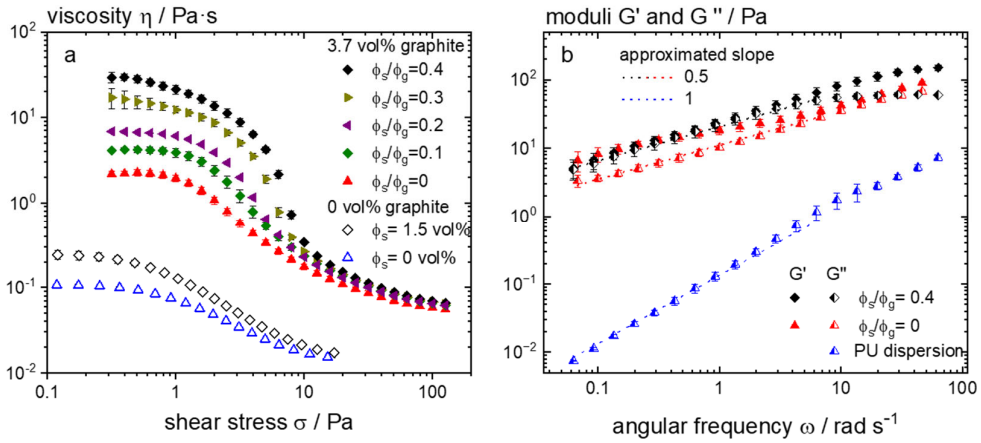

Figure 2. (**a**) Viscosity vs. shear stress σ for a PU dispersion (35 vol% particle loading) without (open symbols) and with 3.7 vol% graphite flakes (closed symbols); the fraction of octanol added to the graphite filled system varied from φ_s/φ_g = 0 to 0.4. The sample with φ_s/φ_g = 0.4 (black closed diamond) has the same ratio of octanol to PU dispersion as the sample without graphite and 1.5 vol% octanol (black open diamond). (**b**) Storage modulus (closed symbols) and loss modulus (half-open symbols) versus angular frequency $\omega = 2\pi f$ for the pure PU dispersion (blue) and selected samples with 3.7 vol% graphite flakes also depicted in a). Note: for the low-viscosity weakly shear thinning PU dispersion, G′ was not accessible since G′ << G″ in the frequency range covered here.

The pure PU dispersion exhibits a weakly shear thinning behavior with a zero-shear viscosity of 0.1 Pa·s, which is typical for an aqueous dispersion of particles stabilized by short-range repulsive interactions, resulting in an effective particle loading $\varphi_{eff} > \varphi$ = 35 vol%. Figure 2b shows the loss modulus in the frequency range corresponding to the Newtonian regime at low shear rates; accordingly, G″ increases linearly with the frequency and G′ is negligibly small in this range. The downturn of the G″ vs. ω curve at the highest measured frequencies indicates the onset of shear thinning. Adding 1.5 vol% octanol, assuming to be emulsified as small droplets in the aqueous phase, roughly results in a twofold increase in the zero-shear viscosity due to the corresponding increase in the disperse-phase volume fraction. As expected, the effect of adding a small fraction of graphite flakes on the viscosity of the PU dispersion is much stronger, due to the high shape anisotropy of the added particles [39] and the suspension including 3.7 vol% graphite flakes without added octanol exhibits a 20fold increase in viscosity compared to the pure PU dispersion. The change occurring with adding graphite flakes is also evident in the frequency sweep. The storage and loss moduli are closely aligned, and both exhibit a similar weak frequency dependence corresponding to a power-law scaling G′, $G'' \approx \omega^{0.5}$ over an extended frequency range typical for a system close to the sol–gel transition point [40]. Adding octanol to this mixture does not have a high impact on the moduli. We observe a slight increase in the storage and loss modulus but a similar frequency dependence. For a capillary suspension exhibiting a percolating particle network, we would expect a storage modulus, which is frequency independent and much higher than the loss modulus, indicating a gel-like state [41]. This behavior as well as the absence of a yield stress indicates

that the characterized samples are below the percolation threshold. Even though octanol has only a weak effect on the linear viscoelastic response of the fluid, its addition has a more pronounced effect on the steady shear viscosity than adding it to the pure PU dispersion and a further 15fold increase in the zero-shear viscosity is observed for the sample with φ_s/φ_g = 0.4, which has the same ratio of octanol to PU dispersion as the pure PU dispersion with 1.5 vol% octanol added. It should be noted that despite its strong effect on the zero-shear viscosity, octanol does not alter the high-shear viscosity of the graphite-filled PU dispersion and at shear stresses $\sigma > 10$ Pa, the flow curves for the samples with different φ_s/φ_g essentially superimpose. Due to the absence of a distinct yield stress and the distinct viscoelastic response, we have to conclude that no sample-spanning particle network is formed in these samples. Nevertheless, the strong increase in low-shear viscosity suggests that large, loosely packed particle aggregates or flocs are formed, which immobilize part of the continuous phase. Apparently, more or larger flocs are formed with the increasing octanol content, but these flocs cannot withstand strong shear forces and disintegrate at high shear stresses according to the superimposing flow curves for $\sigma > 10$ Pa. This is similar to capillary suspensions with their sample-spanning particle network [42].

3.1.2. Effect of Octanol Above Percolation Threshold

To create a percolating particle network, a minimum amount of particles are required depending on their size and shape. Using the occurrence of a yield stress as criterion, we found that more than 22 vol% of the spherical and more than 3.7 vol% of the flake-shaped graphite particles used here are necessary to create a percolating particle network. In this study, octanol was selected as the secondary liquid due to its significant effect on the yield stress. However, samples containing other immiscible liquids, such as paraffin oil and methyl oleate, were also prepared. The incorporation of paraffin oil resulted in a twofold increase in yield stress compared to conventional suspensions, whereas methyl oleate exhibited no measurable effect. The selection of the secondary liquid is nontrivial, mainly governed by factors such as the filler particle wetting behavior, interfacial tension, and here also the swelling of PU nanoparticles by the added secondary liquid. The latter can be excluded for octanol. However, the utilization of other secondary fluids also remains feasible. In Figure 3, the change in the yield stress with the increasing ratio of secondary liquid to graphite volume fraction φ_s/φ_g is shown for PU dispersions including φ_g = 4.5 vol% of particle flakes and φ_g = 28 vol% of spherical particles, respectively. The data were analyzed using consecutive creep tests (stress ramp) and oscillatory shear amplitude sweep measurements, as depicted in the Supplementary Materials section. Considering the yield stress is not an intrinsic material property, but rather a parameter also depending on the type of test and selected test parameters (time scale), the agreement between the results from both tests is good.

In contrast to the sample including flake-shaped graphite particles, the sample prepared with the spherical particles does not exhibit a yield stress without added octanol. Nevertheless, in both cases, a yield stress occurs upon the addition of trace amounts of octanol and σ_y strongly increases with the increasing secondary fluid content and exceeds 100 Pa at φ_s/φ_g = 0.12 for the samples with the spherical and at φ_s/φ_g = 0.4 for the samples including the flake-shaped graphite particles. The slope of the σ_y vs. φ_s/φ_g curves not only depends on the particle shape but also on the particle volume fraction and for the systems selected here, the increase is steeper for the spherical particle system than for the dispersion filled with flake-shaped graphite particles. In the former case, the yield stress starts to drop at φ_s/φ_g = 0.2; this phenomenon has been observed earlier and could be attributed to spherical agglomeration, i.e., the formation of dense particle aggregates surrounded by the better wetting fluid [23]. Using a grindometer [24], the onset of the formation of a

few large aggregates was observed for the sample including 28 vol% spherical graphite particles already at $\varphi_s/\varphi_g = 0.2$. Samples with a higher secondary fluid content included more large agglomerates. It was no longer possible to form homogeneous pastes without further mechanical treatment, e.g., using a three-roll mill; such samples are not suited for making smooth films with uniform distribution of filler particles and were excluded from further investigations.

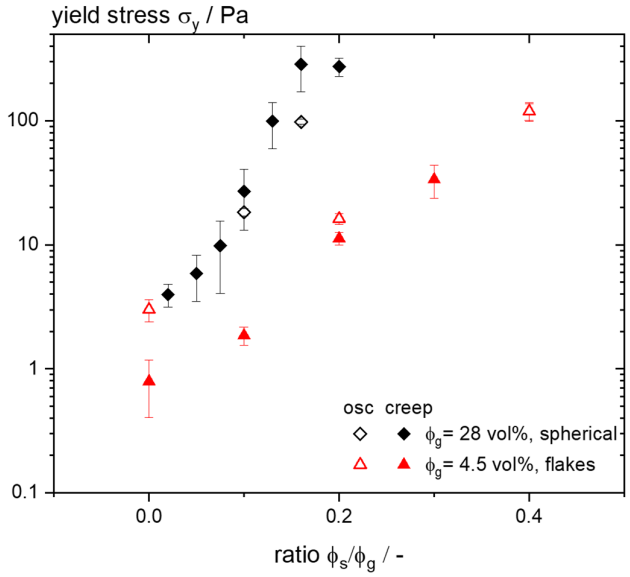

Figure 3. Yield stress σ_y as a function of the ratio of secondary liquid to graphite volume fraction φ_s/φ_g for a PU dispersion filled with 4.5 vol% of flake-shaped particles (red triangles) and 28 vol% of spherical particles (black diamonds) obtained from consecutive creep tests (closed symbols) and via oscillatory stress amplitude sweeps (open symbols) as described in Section 2.4. Error bars include experimental uncertainty of at least three measurements performed on fresh rheometer fillings from one paste preparation as well as error propagation of variations in sample preparation.

By introducing a yield stress, the sedimentation of graphite particles can be slowed down substantially. To demonstrate this, Figure 4 shows samples with different ratios φ_s/φ_g placed in narrow cylindrical test tubes; pictures were taken during a 6-month storage period at room temperature.

The sample without octanol (no yield stress) shows clearly visible sedimentation already after one day. The sedimentation boundary hardly shifts afterward, but the supernatant continues to clarify. In the capillary suspension with a ratio of $\varphi_s/\varphi_g = 0.1$ and $\sigma_y = 27 \pm 14$ Pa, the first signs of sedimentation are visible after two days. After four days, a boundary forms that does not shift further. This boundary is significantly higher than in the sample without octanol. The sample with a ratio of $\varphi_s/\varphi_g = 0.2$ and $\sigma_y = 274 \pm 46$ Pa shows no visually detectable sedimentation at all during the 6-month test period. This demonstrates that sedimentation can be effectively slowed down and the sample shelf life can be extended over several months simply by adding a small fraction of a secondary liquid immiscible with the bulk fluid of the suspension. It should be noted here that models predicting the yield stress necessary to prevent settling in uniform viscoplastic fluids [17] do not necessarily apply to particulate gels [43]. In such gels, the characteristics of the microstructure must be considered and for systems like those investigated here, particles not attached to a large floc or sample-spanning network settle in a low-viscosity continuous phase. The high yield stress necessary to suppress sedimentation for the systems investigated here reflects that particles must be tightly attached to a strong percolating network in order to avoid settling.

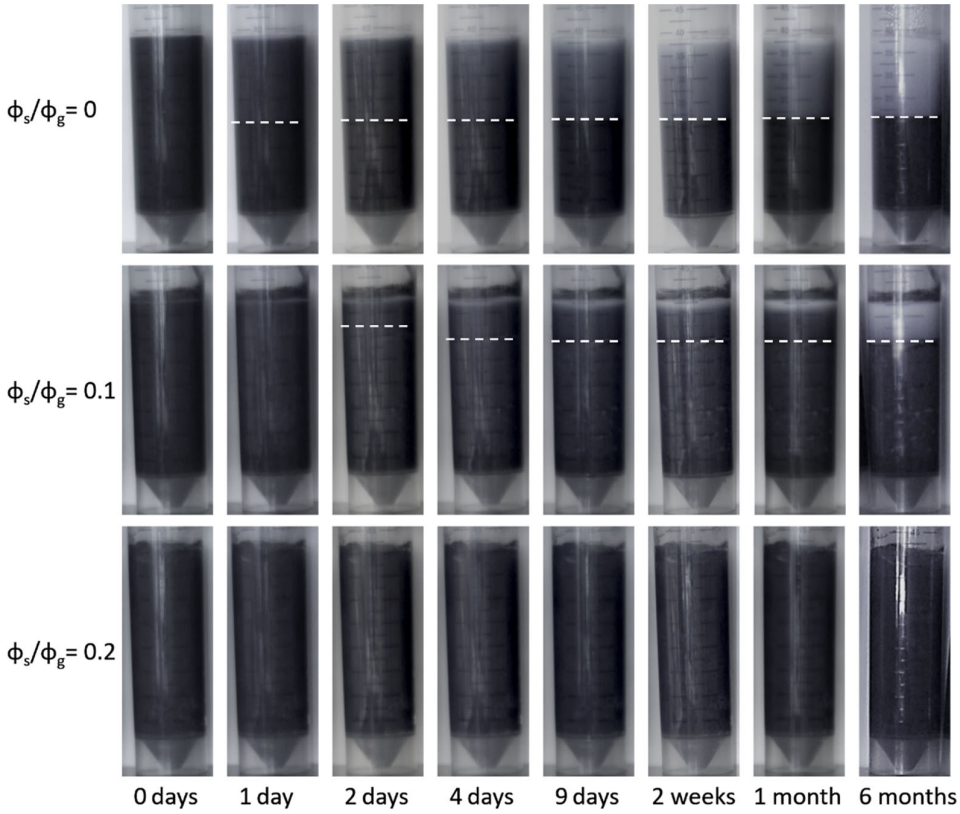

Figure 4. Images of PU dispersion including 28 vol% of spherical particles and different ratios of secondary liquid to particle volume fraction φ_s/φ_g stored in narrow cylindrical test tubes (diameter: 28 mm, length: 93 mm) taken during a 6-month storage period. The dashed line indicates the boundary between sediment and supernatant.

3.1.3. Effect of Hydrophobically Modified Polyether—HMPE Thickener

Section 3.1.1 demonstrated that the capillary suspension concept can be used to significantly increase the low-shear viscosity of graphite-filled PU dispersions, while the viscosity remains essentially unchanged at high shear rates. For many applications, especially coating or printing operations, it is crucial to be able to control the viscosity in this high shear rate range as well [44–46]. In order to adjust the high-shear viscosity of capillary suspensions, the use of additional thickening agents is required. Previous studies have shown that the presence of adsorbing polymers can prevent the formation of capillary suspensions if the secondary liquid does not preferentially wet the particles [47]. Here, samples were prepared using a commercially available associative thickener, to determine whether it is possible to adjust the high-shear viscosity without affecting the particle network. Figure 5 illustrates the impact of an HMPE thickening agent on the flow behavior of the pure PU dispersion, as well as a non-percolating ternary suspension (φ_g = 0.22, φ_s/φ_g = 0.1), a capillary suspension (φ_g = 0.28, φ_s/φ_g = 0.1), as well as the corresponding regular suspension (φ_g = 0.28, φ_s/φ_g = 0) consisting of the PU dispersion filled with spherical graphite particles. Note, the amount of thickener added to the samples without graphite was chosen such that the thickener concentration in the aqueous phase was the same as for the corresponding capillary suspension.

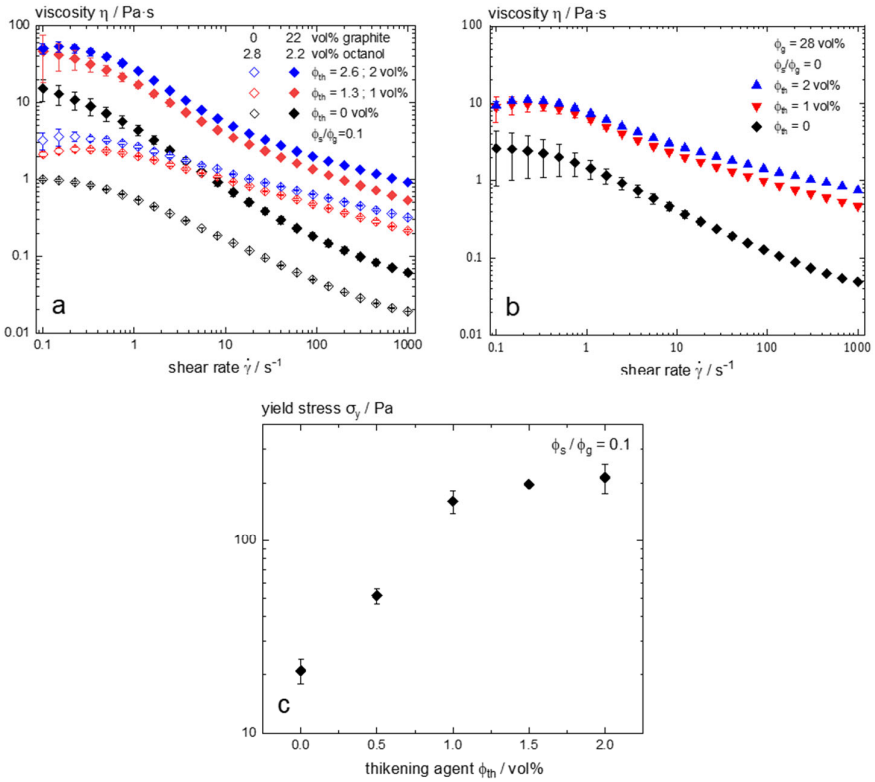

Figure 5. (**a**) Viscosity as a function of shear rate for the PU dispersion filled with 22 vol% spherical graphite and a ratio of $\varphi_s/\varphi_g = 0.1$ with varying amount of thickener (closed symbols) and for samples without graphite with the same concentration of thickener and octanol in the aqueous phase (open symbols); (**b**) viscosity as a function of shear rate for the PU dispersion filled with 28 vol% spherical graphite without octanol ($\varphi_s/\varphi_g = 0$) but varying amount of thickener φ_{th}; (**c**) yield stress vs. volume fraction of thickening agent φ_{th} for the PU dispersion filled with 28 vol% spherical graphite and $\varphi_s/\varphi_g = 0.1$.

In all cases, the impact of the thickener on the viscosity is more pronounced at high shear rates than in the low shear range. For the sample without graphite (PU dispersion + octanol), adding 1.3 vol% thickener (equivalent to φ_{th} = 1 vol% in the capillary suspension) increases the viscosity at $\dot{\gamma}$ = 0.1 s^{-1} by a factor of 2.5, whereas the viscosity increases by about one order of magnitude for $\dot{\gamma}$ = 1000 s^{-1}. Increasing φ_{th} to 2.6 vol% results in a further, but less pronounced increase in the viscosity without a change in the shape of the flow curve. This high thickening efficiency at high shear rates (and low thickener concentration) is in line with the information provided by the manufacturer [48].

As already shown above, the addition of graphite increases the low-shear viscosity distinctly. Adding 22 vol% spherical graphite particles is still below the critical concentration necessary for the self-assembly of a sample-spanning network controlled by capillary forces. In this case, the effect of the thickener is similar as for the samples without graphite. Adding 1 vol% thickener triples the viscosity at low shear rates, while at $\dot{\gamma}$ = 1000 $s^{-1,}$ again, a viscosity increase by about an order of magnitude is observed. As above, further increasing the thickener content to φ_{th} = 2 vol% leads to a further approximately 1.5-fold rise in the viscosity irrespective of the shear rate. These results indicate that thickening essentially takes place in the aqueous phase.

The sample including 28 vol% of spherical graphite particles but without added octanol also does not exhibit a yield stress, and the effect of adding the HMPE thickener is similar as described above; at $\dot{\gamma}$ = 1 $s^{-1,}$ the viscosity increase is 3-fold, but at $\dot{\gamma}$ = 1000 $s^{-1,}$ the viscosity again increases by an order of magnitude when 1 vol% thickener is added.

Adding octanol to this system leads to the formation of a capillary suspension exhibiting a distinct yield stress. As illustrated in Figure 5c for the sample with $\varphi_s/\varphi_g = 0.1$, adding the HMPE thickener has a significant effect on this quantity and σ_y increases almost by an order of magnitude (from 21 ± 3 Pa to 160 ± 21 Pa) when 1 vol% thickener is added, but σ_y levels off for higher thickener concentrations. These results clearly demonstrate that the thickener does not displace the secondary liquid from the particles but additionally stabilizes the particle network. For such materials, we can, of course, not define a low-shear-limiting viscosity; on the other hand, the high-shear viscosity is hard to determine due to experimental limitations of rotational rheometry. The samples with a thickener content $\varphi_{th} \geq 1$ vol% exhibited sample spillage at stresses just exceeding σ_y. High-shear viscosity values could only be obtained for samples with a thickener volume fraction of 0.5 vol% or less. Here, an increase of one order of magnitude in viscosity was observed despite the lower HMPE content compared to the systems discussed above. This further highlights the efficiency of the thickener even in the capillary suspension state and demonstrates its suitability for thickening such particulate gels including nano-scale polymer particles as well as micron-sized graphite particles.

3.2. Graphite-Filled PU Films—Effect of Second Liquid on Film Properties

From the samples discussed in Section 3.1, films were produced, and tensile tests as well as electrical conductivity measurements were performed in order to evaluate whether the change in the microstructure in the wet state due to the added octanol also shows up in the corresponding dry film. The graphite volume fraction given from here on refers to the fraction in the dried film.

3.2.1. Electrical Conductivity

It has been demonstrated for various adhesives and elastomers that the percolation threshold for thermal or electrical conductivity can be drastically lowered using the capillary suspension concept [36,49]. The particle loading of the samples investigated here, however, is well above the percolation threshold and we do not expect a substantial increase in electrical conductivity due to the added octanol, e.g., for the sample including 28 vol% spherical graphite, the particle loading increases to 54 vol% in the corresponding dry film. According to Figure 3, this sample exhibits a yield stress, i.e., a percolating particle network in the wet state when octanol is added, but not without octanol. The conductivity of the corresponding films varies between 28 ± 9 S/m without octanol and 24 ± 1 S/m for $\varphi_s/\varphi_g = 0.2$, i.e., within experimental uncertainty, the secondary liquid has no impact on the conductivity of PU films including spherical graphite particles.

For films made from suspensions including flake-like particles at concentrations below and above the critical particle loading necessary for the formation of a percolating network, the conductivity of the corresponding films is shown in Figure 6a.

It is noteworthy that we observe an increase in electrical conductivity of nearly an order of magnitude between films including 8.9 and 10.9 vol% graphite. This increase corresponds to the formation of a sample-spanning particle network already in the wet paste, as inferred from the data on the apparent viscosity depicted in Figure 5b indicating a yield stress for the samples with $\varphi_g = 4.1$ vol% with and without added octanol. However, the conductivity of the dry films does not vary with φ_s/φ_g, i.e., the fraction of added octanol; the corresponding formation of particle aggregates at $\varphi_g = 3.3$ vol% and a percolating particle network at $\varphi_g = 4.1$ vol%, coming with a drastic increase in yield stress (similar as shown in Figure 3 in the latter case, have no effect on the electrical conductivity of these films including flake-shaped graphite particles. The absolute values of the conductivity are in a similar range as the literature. Novák showed a conductivity of max. 0.3 S/m for a graphite–

PU composite [14] and Zou reached a conductivity of 1 S/m for a graphite/polystyrene composite [50]. The variations with φ_s/φ_g are within experimental uncertainty considering the error propagation from variations in sample preparation.

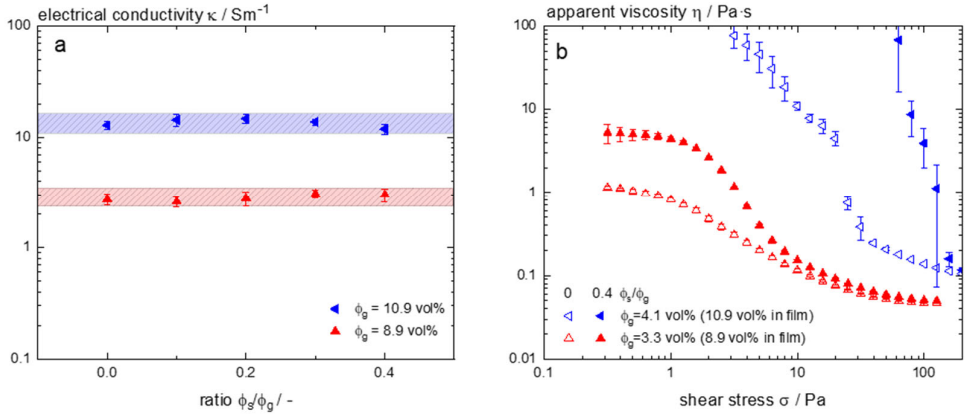

Figure 6. (**a**) Electrical conductivity as a function of the ratio of secondary liquid to graphite volume fraction for different volume fractions φ_g of flake-shaped graphite particles; (**b**) apparent viscosity as a function of shear stress without octanol (open symbols) and with a secondary liquid to graphite volume fraction φ_s/φ_g = 0.4 (closed symbols) for the corresponding wet pastes with graphite volume fractions φ_g corresponding to the values for the dry films shown in (**a**). Note, the term apparent viscosity is used here, because it is not clear whether the viscosity data for the samples with φ_g = 4.1 vol% determined at stresses just above the yield stress refer to a uniform shear deformation within the sample.

3.2.2. Mechanical Properties

The polyurethane film derived from the dispersion without additives exhibits an elastic modulus of 88 ± 32 N/mm^2. It shows a highly ductile behavior, and due to the limitations of our tensile tester, the tensile strength fracture could not be observed, but a lower limit of 11.7 ± 1.2 N/mm^2 could be estimated. Further insights into the tensile test behavior are illustrated in Figure S2, provided as Supplementary Material. With the addition of graphite, the samples exhibit a brittle fracture. The results of the tensile tests are summarized in Table 2. Notably, the samples with spherical and flake-shaped particles exhibit similar Young's moduli, but the films including the flake-shaped particles show increased tensile strength; the latter films are less brittle due to the lower graphite content but nevertheless exhibit a high modulus due to the shape anisotropy and the different microstructure in the film [51]. The secondary liquid seems to have a weak systematic effect, increasing the modulus and decreasing the tensile strength, but the variations are only slightly larger than the experimental uncertainty and more measurements would be required to confirm that. From a technical point of view, these changes are considered not to be relevant.

Table 2. Young's modulus and tensile strength in dependence of the ratio of secondary liquid to graphite volume fraction φ_s/φ_g.

	Young's Modulus [N/mm^2]			**Tensile Strength [N/mm^2]**		
ratio φ_s/φ_g	0	0.1	0.2	0	0.1	0.2
spherical, 54 vol% graphite	270 ± 52	270 ± 45	352 ± 9	5.1 ± 0.3	6.5 ± 1	5.8 ± 1.4
flakes, 11.9 vol% graphite	280 ± 36	245 ± 18	330 ± 24	10.3 ± 0.4	9.8 ± 0.5	9.4 ± 0.3

4. Conclusions

Creating stable suspensions of micron-sized particles in low-viscosity fluids such as polymer dispersions is a challenge when the density difference between the particles and continuous phase is high. In this study, we demonstrate that graphite particles suspended in aqueous PU dispersions can be stabilized against sedimentation using the capillary suspension concept. Both spherical and flake-shaped graphite particles were used as fillers, and octanol, which preferentially wets these particles, was used as the secondary liquid. The addition of octanol leads to a strong, more than 10fold increase in the low-shear viscosity at low graphite particle loadings, which is attributed to the formation of loose particle aggregates immobilizing part of the continuous phase. Above a critical graphite particle concentration, a sample-spanning particle network self-assembles controlled by capillary forces. This is confirmed by a distinct yield stress of these suspensions strongly increasing to values $\sigma_y > 100$ Pa with increasing φ_s/φ_g. Spherical agglomeration sets in when the pendular bridges are oversaturated and large aggregates prevent the formation of uniform dry films from pastes with $\varphi_s/\varphi_g > 0.2$. Sedimentation could be efficiently suppressed for systems showing a percolating particle network and a shelf life of at least 6 months could be achieved.

The capillary suspension concept can be used not only to prevent settling but also to adjust the flow behavior of the suspensions at low shear stresses or shear rates in a wide range. In contrast, at high shear rates, the viscosity curves obtained for different secondary liquid to graphite volume fraction φ_s/φ_g superimpose. However, the viscosity at high shear rates can be efficiently adjusted according to processing or application demands using a hydrophobically modified polyether (HMPE) thickener. The effect of the thickener was investigated for non-percolating systems with spherical particles and octanol, as well as for a percolating system and the corresponding suspension without octanol. The increase in viscosity at high shear rates is similar in all cases. Apparently, thickening essentially takes place in the aqueous phase. The thickener appears to strengthen and stabilize percolating particle networks formed upon the addition of octanol, as can be inferred from the strong increase in yield stress. Films have been prepared from the stabilized suspensions and it could be shown that the electrical conductivity remains unchanged upon the variation in φ_s/φ_g. Changes in the mechanical strength observed due to the added octanol turned out to be small and do not appear to be technically relevant.

This study demonstrates that the capillary suspension concept can be used to prevent the settling of micron-sized, high-density particles in low-viscosity, aqueous polymer dispersions, providing a shelf life of several months. The presence of the nano-scale polymer particles does not disturb the formation of loose aggregates or percolating networks of micron-sized particles controlled by capillary forces. The results presented here have been obtained for graphite particles suspended in a PU dispersion, but a transfer of the concept to other particle systems, such as silver, copper, or metal oxide particles or other polymer systems such as acrylate or rubber dispersions, is straightforward.

Supplementary Materials: The following supporting information can be downloaded at: https://www.mdpi.com/article/10.3390/colloids9030026/s1, Figure S1: Storage modulus G′ and loss modulus G″ vs. shear stress amplitude (a) for spherical particles with a graphite content of φ_g = 28 vol% and different secondary liquid to graphite volume fraction φ_s/φ_g (b) for flake shaped particles with a graphite content of φ_g = 4.5 vol% and different secondary liquid to graphite volume fraction φ_s/φ_g; Figure S2: Stress strain diagrams obtained from tensile tests on (a) the pure PU dispersion (b) to (d) samples with 11.9 vol% graphite flakes and varying secondary liquid to graphite volume fraction φ_s/φ_g and (e) to (g) samples with 54 vol% spherical graphite particles and varying secondary liquid to graphite volume fraction φ_s/φ_g.

Author Contributions: K.D.: Investigation, writing—original draft; N.W.: writing—review and editing, supervision, funding acquisition. All authors have read and agreed to the published version of the manuscript.

Funding: This research received no external funding.

Data Availability Statement: The original contributions presented in this study are included in the article/Supplementary Material. Further inquiries can be directed to the corresponding author.

Acknowledgments: We would like to thank Jonas Kaltenbach for the work at the SEM-microscope and Klaus Hirsch for the particle size analysis. We acknowledge experimental support from Aurelia Kuhn, Niklas Schumacher, and Yuan Yu.

Conflicts of Interest: The authors declare no conflicts of interest.

Abbreviations

The following abbreviations are used in this manuscript:

PU	polyurethane
VOC	volatile organic compounds
HEUR	hydrophobically modified polyurethane
HMPE	hydrophobically modified polyether
LVE	linear viscoelastic range

References

1. Kim, B.K. Aqueous polyurethane dispersions. *Colloid Polym. Sci.* **1996**, *274*, 599–611. [CrossRef]
2. Tielemans, M.; Roose, P. Study of the rheology of aqueous radiation curable polyurethane dispersions modified with associative thickeners. *Prog. Org. Coat.* **2008**, *63*, 182–188. [CrossRef]
3. Chinwanitcharoen, C.; Kanoh, S.; Yamada, T.; Hayashi, S.; Sugano, S. Preparation of aqueous dispersible polyurethane: Effect of acetone on the particle size and storage stability of polyurethane emulsion. *J. Appl. Polym. Sci.* **2004**, *91*, 3455–3461. [CrossRef]
4. Sardon, H.; Irusta, L.; Fernández-Berridi, M.J.; Luna, J.; Lansalot, M.; Bourgeat-Lami, E. Waterborne polyurethane dispersions obtained by the acetone process: A study of colloidal features. *J. Appl. Polym. Sci.* **2011**, *120*, 2054–2062. [CrossRef]
5. Nobel, M.; Picken, S.; Mendes, E. Waterborne nanocomposite resins for automotive coating applications. *Prog. Org. Coat.* **2007**, *58*, 96–104. [CrossRef]
6. Pieters, K.; Mekonnen, T.H. Progress in waterborne polymer dispersions for coating applications: Commercialized systems and new trends. *RSC Sustain.* **2024**, *2*, 3704–3729. [CrossRef]
7. Afridi, M.; Ohama, Y.; Demura, K.; Iqbal, M. Development of polymer films by the coalescence of polymer particles in powdered and aqueous polymer-modified mortars. *Cem. Concr. Res.* **2003**, *33*, 1715–1721. [CrossRef]
8. Yang, C.; Lin, W.; Li, Z.; Zhang, R.; Wen, H.; Gao, B.; Chen, G.; Gao, P.; Yuen, M.M.F.; Wong, C.P. Water-Based Isotropically Conductive Adhesives: Towards Green and Low-Cost Flexible Electronics. *Adv. Funct. Mater.* **2011**, *21*, 4582–4588. [CrossRef]
9. Urban, D.; Takamura, K. *Polymer Dispersions and Their Industrial Applications*; John Wiley & Sons Inc.: Weinheim, Germany, 2002. [CrossRef]
10. Li, Z.; Zhang, R.; Moon, K.; Liu, Y.; Hansen, K.; Le, T.; Wong, C.P. Highly Conductive, Flexible, Polyurethane-Based Adhesives for Flexible and Printed Electronics. *Adv. Funct. Mater.* **2013**, *23*, 1459–1465. [CrossRef]
11. Mehvari, S.; Goodhew, B.; González, S.; Lafdi, K.; Sanchez-Vicente, Y. Effect of processing methods on the electrical conductivity properties of silver-polyurethane composite films (Experimental and numerical studies). *J. Compos. Mater.* **2023**, *57*, 4409–4422. [CrossRef]
12. Wikaramasinghe, G.C.; Manamendra, R.M.; Manuda, K.R.J.; Nissanka, B.; Weerawarne, D.L.; Jayasundara, D.R. Binder-free conductive graphite coatings on polyimide substrates for applications in flexible electronics. *J. Coat. Technol. Res.* **2025**, *22*, 825–838. [CrossRef]
13. Zulfiqar, M.H.; Hassan, M.U.; Maqbool, K.Q.; Mehmood, M.Q.; Riaz, K.; Massoud, Y. Customizable Graphite-On-Paper-Based Keypads: Toward Disposable and Recyclable Wireless Human–Machine Interfaces. *IEEE J. Flex. Electron.* **2023**, *2*, 25–33. [CrossRef]
14. Novák, I.; Krupa, I.; Chodák, I. Investigation of the correlation between electrical conductivity and elongation at break in polyurethane-based adhesives. *Synth. Met.* **2002**, *131*, 93–98. [CrossRef]
15. Bhavsar, R.A.; Nehete, K.M. Rheological approach to select most suitable associative thickener for water-based polymer dispersions and paints. *J. Coat. Technol. Res.* **2019**, *16*, 1089–1098. [CrossRef]

16. Orgilés-Calpena, E.; Arán-Aís, F.; Torró-Palau, A.M.; Orgilés-Barceló, C.; Martín-Martínez, J.M. Influence of the Chemical Structure of Urethane-Based Thickeners on the Properties of Waterborne Polyurethane Adhesives. *J. Adhes.* **2009**, *85*, 665–689. [CrossRef]
17. Balmforth, N.J.; Frigaard, I.A.; Ovarlez, G. Yielding to Stress: Recent Developments in Viscoplastic Fluid Mechanics. *Annu. Rev. Fluid Mech.* **2014**, *46*, 121–146. [CrossRef]
18. Beris, A.N.; Tsamopoulos, J.A.; Armstrong, R.C.; Brown, R.A. Creeping motion of a sphere through a Bingham plastic. *J. Fluid Mech.* **1985**, *158*, 219–244. [CrossRef]
19. Tabuteau, H.; Coussot, P.; de Bruyn, J.R. Drag force on a sphere in steady motion through a yield-stress fluid. *J. Rheol.* **2007**, *51*, 125–137. [CrossRef]
20. Koos, E.; Willenbacher, N. Capillary Forces in Suspension Rheology. *Science* **2011**, *331*, 897–900. [CrossRef]
21. Velankar, S.S. A non-equilibrium state diagram for liquid/fluid/particle mixtures. *Soft Matter* **2015**, *11*, 8393–8403. [CrossRef]
22. Domenech, T.; Velankar, S. Capillary-driven percolating networks in ternary blends of immiscible polymers and silica particles. *Rheol. Acta* **2014**, *53*, 593–605. [CrossRef]
23. Maurath, J.; Bitsch, B.; Schwegler, Y.; Willenbacher, N. Influence of particle shape on the rheological behavior of three-phase non-brownian suspensions. *Colloids Surfaces A Physicochem. Eng. Asp.* **2016**, *497*, 316–326. [CrossRef]
24. Yüce, C.; Okamoto, K.; Karpowich, L.; Adrian, A.; Willenbacher, N. Non-volatile free silver paste formulation for front-side metallization of silicon solar cells. *Sol. Energy Mater. Sol. Cells* **2019**, *200*, 110040. [CrossRef]
25. Aal, K.A.; Willenbacher, N. Front side metallization of silicon solar cells—A high-speed video imaging analysis of the screen printing process. *Sol. Energy Mater. Sol. Cells* **2020**, *217*, 110721. [CrossRef]
26. Roh, S.; Parekh, D.P.; Bharti, B.; Stoyanov, S.D.; Velev, O.D. 3D Printing by Multiphase Silicone/Water Capillary Inks. *Adv. Mater.* **2017**, *29*, 1701554. [CrossRef]
27. Ding, H.; Barg, S.; Derby, B. Direct 3D printing of graphene using capillary suspensions. *Nanoscale* **2020**, *12*, 11440–11447. [CrossRef]
28. Nider, S.; De Ceulaer, F.; Göksel, B.; Braem, A.; Koos, E. Tricalcium phosphate-based capillary suspensions as inks for 3D printing of porous scaffolds. *Open Ceram.* **2025**, *21*, 100744. [CrossRef]
29. Tyowua, A.T.; Harbottle, D.; Binks, B.P. 3D printing of Pickering emulsions, Pickering foams and capillary suspensions—A review of stabilization, rheology and applications. *Adv. Colloid Interface Sci.* **2024**, *332*, 103274. [CrossRef]
30. Bitsch, B.; Dittmann, J.; Schmitt, M.; Scharfer, P.; Schabel, W.; Willenbacher, N. A novel slurry concept for the fabrication of lithium-ion battery electrodes with beneficial properties. *J. Power Sources* **2014**, *265*, 81–90. [CrossRef]
31. Park, J.; Ahn, K.H. Controlling Drying Stress and Mechanical Properties of Battery Electrodes Using a Capillary Force-Induced Suspension System. *Ind. Eng. Chem. Res.* **2021**, *60*, 4873–4882. [CrossRef]
32. Feichtinger, A.; Jarray, A.; Bouwman, W.G.; Duif, C.P.; Valverde-Ayllon, M.C.; Heerkens, K.; Rooijakkers, R.; Landman, J.; Scholten, E. Biopolymer-based capillary suspensions: Influence of particle properties on network formation. *Food Hydrocoll.* **2025**, *163*, 111061. [CrossRef]
33. Han, C.; Wang, G.; Feng, G.; Wang, J.; Guo, J.; Yang, X. Capillary force-driven formation of native starch granule oleogels for 3D printing. *Food Hydrocoll.* **2023**, *150*, 109725. [CrossRef]
34. Menne, D.; da Silva, L.L.; Rotan, M.; Glaum, J.; Hinterstein, M.; Willenbacher, N. Giant Functional Properties in Porous Electroceramics through Additive Manufacturing of Capillary Suspensions. *ACS Appl. Mater. Interfaces* **2022**, *14*, 3027–3037. [CrossRef] [PubMed]
35. Tedjokusuma, K.; Lauth, W.; Willenbacher, N. Manufacture and filtration performance of glass filters made from capillary suspensions. *Sep. Purif. Technol.* **2024**, *329*, 125097. [CrossRef]
36. Sun, H.; Zhang, X.; Yuen, M.M. Enhanced conductivity induced by attractive capillary force in ternary conductive adhesive. *Compos. Sci. Technol.* **2016**, *137*, 109–117. [CrossRef]
37. Zhang, Y.; Allen, M.C.; Zhao, R.; Deheyn, D.D.; Behrens, S.H.; Meredith, J.C. Capillary Foams: Stabilization and Functionalization of Porous Liquids and Solids. *Langmuir* **2015**, *31*, 2669–2676. [CrossRef]
38. Mezger, T.G. *Das Rheologie-Handbuch: Für Anwender von Rotations- und Oszillations-Rheometern*, 3rd ed.; Vincentz Network: Hannover, Germany, 2010; ISBN 978-3-86630-863-3.
39. Brenner, H. Rheology of a dilute suspension of axisymmetric Brownian particles. *Int. J. Multiph. Flow* **1974**, *1*, 195–341. [CrossRef]
40. Winter, H.H.; Mours, M. Rheology of Polymers Near Liquid-Solid Transitions. In *Neutron Spin Echo Spectroscopy Viscoelasticity Rheology*; Springer: Berlin/Heidelberg, Germany, 1997; pp. 165–234. [CrossRef]
41. Koos, E. Capillary suspensions: Particle networks formed through the capillary force. *Curr. Opin. Colloid Interface Sci.* **2014**, *19*, 575–584. [CrossRef]
42. Koos, E.; Johannsmeier, J.; Schwebler, L.; Willenbacher, N. Tuning suspension rheology using capillary forces. *Soft Matter* **2012**, *8*, 6620–6628. [CrossRef]

43. Emady, H.; Caggioni, M.; Spicer, P. Colloidal microstructure effects on particle sedimentation in yield stress fluids. *J. Rheol.* **2013**, *57*, 1761–1772. [CrossRef]
44. Luo, Y.; Le Fer, G.; Dean, D.; Becker, M.L. 3D Printing of Poly(propylene fumarate) Oligomers: Evaluation of Resin Viscosity, Printing Characteristics and Mechanical Properties. *Biomacromolecules* **2019**, *20*, 1699–1708. [CrossRef] [PubMed]
45. Teng, W.D.; Edirisinghe, M.J.; Evans, J.R.G. Optimization of Dispersion and Viscosity of a Ceramic Jet Printing Ink. *J. Am. Ceram. Soc.* **1997**, *80*, 486–494. [CrossRef]
46. Cisneros-Zevallos, L.; Krochta, J. Dependence of Coating Thickness on Viscosity of Coating Solution Applied to Fruits and Vegetables by Dipping Method. *J. Food Sci.* **2003**, *68*, 503–510. [CrossRef]
47. Bitsch, B.; Braunschweig, B.; Willenbacher, N. Interaction between Polymeric Additives and Secondary Fluids in Capillary Suspensions. *Langmuir* **2016**, *32*, 1440–1449. [CrossRef]
48. BASF SE. Formulation Challenges and Product Recommendations. Available online: https://www.basf.com/dam/jcr:fa3b3f34-94a5-3340-a992-680219cd5c90/basf/www/global/segments/industrial-solution/BASF%20Rheology%20Modifiers%20Product%20Recomendation(AP).pdf (accessed on 13 February 2025).
49. Sun, H.; Han, Z.; Willenbacher, N. Ultrastretchable Conductive Elastomers with a Low Percolation Threshold for Printed Soft Electronics. *ACS Appl. Mater. Interfaces* **2019**, *11*, 38092–38102. [CrossRef]
50. Zou, J.; Yu, Z.; Pan, Y.; Fang, X.; Ou, Y. Conductive mechanism of polymer/graphite conducting composites with low percolation threshold. *J. Polym. Sci. Part B Polym. Phys.* **2002**, *40*, 954–963. [CrossRef]
51. Eichner, E.; Heinrich, S.; Schneider, G. Influence of particle shape and size on mechanical properties in copper-polymer composites. *Powder Technol.* **2018**, *339*, 39–45. [CrossRef]